Photoinduced States in a Mott Insulator

Martin Eckstein[1] and Philipp Werner[2]
[1]Max Planck Research Department for Structural Dynamics, University of Hamburg-CFEL, 22761 Hamburg, Germany
[2]Department of Physics, University of Fribourg, 1700 Fribourg, Switzerland
(Received 11 July 2012; published 18 March 2013)

We investigate the properties of the metallic state obtained by photodoping carriers into a Mott insulator. In a strongly interacting system, these carriers have a long lifetime, so that they can dissipate their kinetic energy to a phonon bath. In the relaxed state, the scattering rate saturates at a nonzero temperature-independent value, and the momentum-resolved spectral function features broad bands which differ from the well-defined quasiparticle bands of a chemically doped system. Our results indicate that a photodoped Mott insulator behaves as a bad metal, in which strong scattering between doublons and holes inhibits Fermi-liquid behavior down to low temperature.

DOI: 10.1103/PhysRevLett.110.126401 PACS numbers: 71.10.Fd

Carrier doping provides a convenient way of controlling the properties of strongly correlated materials. The high-T_c cuprates, e.g., undergo a doping-driven transition from an antiferromagnetic Mott insulator to a correlated metal that becomes superconducting at low temperatures. While doping is usually achieved by modifying the chemical composition of a material, photodoping, i.e., a change of the electron and hole concentrations by irradiating light on a sample, provides a straightforward way to influence material properties in an ultrafast manner. Photoinduced insulator-to-metal transitions have been demonstrated in organic materials [1,2], charge-transfer insulators [3], and cuprates [4].

In contrast to chemically doped states, photodoped states simultaneously have electron and hole-like carriers, and these carriers are typically inserted with large kinetic energy. In a semiconductor, this mainly results in a different occupation of valence and conduction bands, which themselves are rigid, i.e., independent of filling and temperature. In contrast, the formation of a Fermi liquid in a doped correlated system leads to a narrow band of delocalized quasiparticle states without any counterpart in the insulator. Because these quasiparticles are strongly damped at high temperature, and because the adiabatic correspondence between bare electrons and quasiparticle excitations of a Fermi liquid is anyway difficult to reconcile with the presence of both holes and electrons, the properties of a correlated photodoped state are not obvious. Its large kinetic energy works against correlations and could cause a rigid-band behavior. On the other hand, lifetimes of a few picoseconds indicate that carriers are strongly coupled to spin fluctuations or phonons [3,4]. They might thus dissipate their energy before recombination and reveal correlation effects in a photodoped state and possible differences to a Fermi liquid.

In this Letter, we contrast photodoped and chemically doped Mott insulators in the simplest possible setup, which is a paramagnetic single-band Mott insulator that is initially perturbed by an intense laser pulse. For this purpose we focus on the Hubbard model

$$H = -v \sum_{\langle ij\rangle,\sigma=\uparrow,\downarrow} c^{\dagger}_{i\sigma} c_{j\sigma} + U \sum_i n_{i\uparrow} n_{i\downarrow} - \mu \sum_{i\sigma} n_{i\sigma}, \quad (1)$$

which describes electrons that hop (with amplitude v) between nearest neighbors $\langle ij\rangle$ of an infinite crystal lattice and interact through a local Coulomb repulsion U. The electric field of the laser pump is determined by the vector potential $\boldsymbol{E} = -\frac{1}{c}\partial_t \boldsymbol{A}$, which in turn enters Eq. (1) by the Peierls substitution; i.e., band energies $\epsilon_{\boldsymbol{k}}$ are shifted to $\tilde{\epsilon}_{\boldsymbol{k}} = \epsilon_{\boldsymbol{k}-ea/\hbar c \boldsymbol{A}(t)}$ (see, e.g., Ref. [5]). If the Mott gap is large ($U \gg v$), electron-hole pairs have a long lifetime, because the electronic decay channel involving a direct conversion of interaction energy into kinetic energy becomes inefficient [6]. To account for dissipation of energy to other degrees of freedom, we weakly couple our model to a bosonic bath.

The model is treated within the nonequilibrium extension [7,8] of dynamical mean-field theory (DMFT) [9], which has recently been applied to a quite diverse set of problems in nonequilibrium strongly correlated systems [10–14]. A direct way to incorporate dissipation into this formalism is to attach one particle reservoir to each lattice site [10,14,15]. Here we instead use baths of harmonic oscillators, such that the particle number remains constant while energy is exchanged with the environment. The electronic self-energy, which is a functional of the local Green function G in DMFT, is then the sum of the electronic contribution $\Sigma_U[G]$ and a bath contribution. Vertex corrections are neglected for weak coupling to the bath. The bath contribution is the lowest order diagram for a Holstein-type electron-phonon coupling, $\Sigma_{\mathrm{diss}}[G] = \lambda^2 G(t,t')D(t,t')$, where λ measures the coupling strength and $D(t,t')$ is the equilibrium propagator for a boson with energy ω_0 at given temperature $1/\beta$ (such that the bath has no memory); following the notation of Ref. [16]

for contour-ordered Keldysh Green functions, $D(t,t') = -i\mathrm{Tr}[T_C \exp(-i\int_C dt\omega_0 b^\dagger b) b(t) b^\dagger(t')]/Z$ ($\omega_0 = v$ in the following).

Local diagrams for $\Sigma_U[G]$ are summed to all orders by solving an auxiliary single-impurity Anderson problem, for which we will use the self-consistent strong-coupling expansion [17]. The resulting equations have been explained in Ref. [18]. To include dissipation we replace the band energy $\tilde{\epsilon}_k$ by $\tilde{\epsilon}_k + \Sigma_{\mathrm{diss}}[G]$ in those equations. To access the long time scale $\propto 1/\lambda^2 \gg 1$ associated with dissipation, we are mostly restricted to the lowest order of the strong-coupling expansion, the noncrossing approximation (NCA) [19]. While it is known that NCA fails at low temperatures (leading to noncausal behavior or an unstable time evolution in nonequilibrium), such artifacts do not affect our work, because our main results are obtained for a (doped) Mott insulator at $U \gg v$, above and close to the Fermi-liquid coherence temperature, where the use of NCA is still justified ($U = 14v$, as for the organic salt ET-F_2TCNQ). Corrections from higher order diagrams in the strong-coupling expansion can be considered for somewhat shorter times, but they do not affect our conclusions (see Supplemental Material [20]).

DMFT is exact for infinite dimensions [21] and yields the generic behavior of a high-dimensional lattice, independent of the lattice geometry used within the calculation (mainly, the energy scales are renormalized for different geometries). In this Letter, we perform all calculations for the paramagnetic phase of a one-dimensional system, because this drastically simplifies the momentum summations, but we expect the results to be representative of high-dimensional systems (Supplemental Material [20]). The van Hove singularities of the band edges, which are particular to the one-dimensional case, appear far from the Fermi surface and are thus blurred by the self-energy for $U \gg v$ both at and close to half filling. The unit of energy is set by the hopping v, and time is measured in units of $\hbar/v$. In these units, the critical end point of the first-order Mott transition line for the half-filled system is located at $U \approx 4$–5. The pump pulse $E(t) = E_0 \sin[\Omega(t-t_0)] \times \exp[-4.605 \times (t-t_0)^2/t_0^2]$ is taken to be a sine wave with frequency Ω, amplitude E_0, and a Gaussian envelope. The number of cycles, $N = t_0\Omega/\pi$, is taken between 2 and 10 below. To analyze photodoped and equilibrium states, we compute the real-time optical conductivity [22] and its partial Fourier transform: $\sigma(\omega,t) = \int_0^{s_{\max}} ds \sigma(t, t-s) e^{i\omega s}$. We also define an average of $\sigma(\omega, t)$ which is more local in time and frequency (and almost independent of the cutoff $s_{\max} = t$):

$$\bar{\sigma}(\omega, t; \Delta) \equiv \int_0^{s_{\max}} ds e^{-s^2\Delta^2/2} \sigma(t, t-s) e^{i\omega s}, \qquad (2)$$

equivalent to broadening $\sigma(\omega, t)$ with $\exp(-\omega^2/2\Delta^2)$.

Before studying the photodoped case, we investigate the influence of the dissipative bath on equilibrium properties of the (doped) Mott insulator. Pronounced bath-induced artifacts begin to appear for $\lambda \gtrsim 0.8$, as exemplified for the spectral function of the insulating phase in Fig. 1(a). Because our approximation is only suitable for weak coupling between electrons and bath, we will from now on restrict λ to values where those features are absent and dissipation implies only a slight broadening of the spectrum ($\lambda \lesssim 0.6$). Small electron doping ($n > 1$) of the Mott insulator leads to the formation of a narrow quasiparticle peak at the lower edge of the upper Hubbard band, which goes along with the emergence of a Drude peak in the low-frequency part of the optical conductivity [Fig. 1(b)], $\sigma(\omega) = D\gamma\pi^{-1}[\gamma^2 + \omega^2]^{-1} + \sigma_{\mathrm{incoh}}(\omega)$. For a Fermi liquid, the scattering rate γ decreases with decreasing temperature, with the asymptotic behavior $\gamma \sim T^2$. Although the NCA approximation is known to suffer from noncausal artifacts deep in the Fermi liquid regime, the onset of this Fermi liquid regime can still be observed around $\beta = 20$, by extracting γ from a fit of $\sigma(\omega)$ with a Lorentz curve (Fig. 1, inset). For $\beta \lesssim 20$, coupling to a bath with $\lambda = 0.6$ has only a small influence on the scattering rate.

In the following paragraphs, we study the relaxation of the double occupancy and kinetic energy [Figs. 2(a)–2(f)] after a pump at $\Omega = U$ has created a small number of charge excitations in the system. Without dissipation ($\lambda = 0$) and for small U ($U = 4$, 5), both $d(t)$ and $E_{\mathrm{kin}}(t)$ follow an exponential relaxation $d(t) \sim d_\infty + Ae^{-t/\tau}$ towards a value $d_\infty \neq d(0)$. This fact has already been described for the hypercubic lattice in Ref. [18], where it was also verified that d_∞ is consistent with a thermalization of the system at a temperature that is determined by the total amount of absorbed energy. The thermalization time exponentially increases with U [Fig. 2(h)], in agreement with the predicted exponentially long lifetime of doublons in the Hubbard model for $U \gg v$ [6]. In the insulator

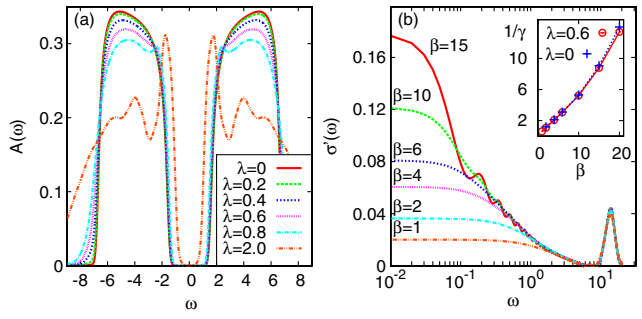

FIG. 1 (color online). (a) Equilibrium spectral function of the half-filled insulator for $U = 8$, $\beta = 10$, and various λ. (b) Frequency-dependent conductivity $\sigma(\omega)$ of the doped Mott insulator at various temperatures, $U = 14$, $n = 1.02$. Fourier artifacts due to a finite cutoff $s_{\max} = 40$ appear when the peak becomes too narrow ($\beta = 15$). The inset shows the Drude relaxation time $1/\gamma$, obtained from a Lorentzian fit to $\sigma(\omega)$ for $0 < \omega < 0.2$.

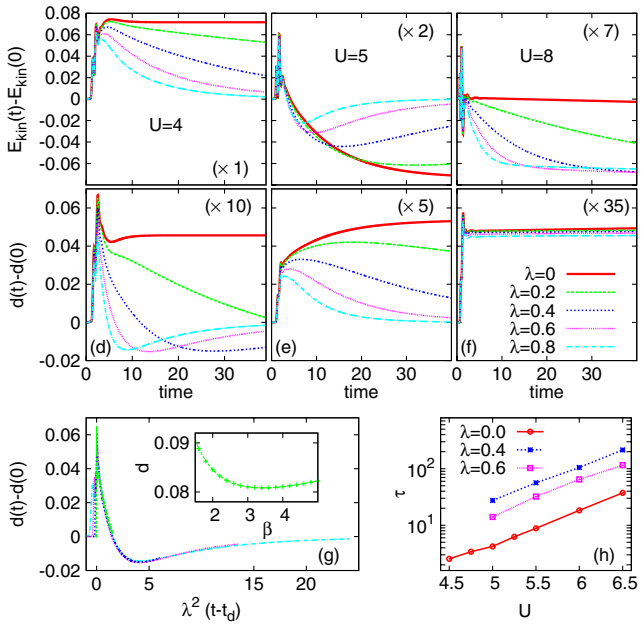

FIG. 2 (color online). Relaxation of the kinetic energy (a)–(c) and double occupancy (d)–(f) for $U = 4$ (left), $U = 5$ (middle), and $U = 8$ (right), during and after a pump with frequency $\Omega = U$, $N = 10$ cycles, $E_0 = 1$; $\beta = 10$. The curves show the differences to the initial state values, brought to the same scale by an additional factor ("×"). Bold solid lines correspond to no dissipation. (g) The same data as (d), plotted against rescaled time $t' = \lambda^2(t - t_d)$, where t_d is the duration of the pump. The inset shows the equilibrium value of d as a function of β for $U = 4$. (h) Relaxation time of the double occupancy, extracted from an exponential fit.

($U = 8$), τ becomes so large that $d(t)$ and $E_{\mathrm{kin}}(t)$ remain constant on the scale of the plot, apart from a short initial transient.

Dissipation completely modifies this picture: Instead of approaching a thermal equilibrium value at higher temperature, both $d(t)$ and $E_{\mathrm{kin}}(t)$ now relax back to their initial values for $U = 4$ and $U = 5$. For $U = 4$, this process can be understood within a two-temperature picture [23]: Because the electronic thermalization time is only a few $\hbar/v$ [Fig. 2(h)], electrons can reach a quasiequilibrium state at high temperature T^* before energy is transferred to the environment. The temperature T^* is subsequently reduced towards the fixed temperature of the bath with a rate entirely determined by λ. This interpretation is supported by the observation that the curves $d(t) - d(0)$ for $U = 4$ fall on top of each other when the time axis is rescaled by λ^2 [Fig. 2(g)], indicating a passage through the same sequence of equilibrium states. In fact, because $U = 4$ is in the metal-insulator crossover region, the double occupancy behaves nonmonotonically as a function of temperature [inset in Fig. 2(g)], which explains the minimum in $d(t)$.

Because the energy quantum that can be transferred to the bath is limited ($\omega_0 = v$), coupling to the bosons does not open an efficient channel for the doublon decay for $U \gg v$. Consequently, the relaxation rate of the double occupancy to its initial value shows a similar exponential increase with U as the thermalization time for $\lambda = 0$ [Fig. 2(h)], and the bath has no effect on $d(t)$ in the insulator ($U = 8$). The kinetic energy, however, does relax to a value that is lower than after the excitation, indicating that doublons and holes are cooled to the temperature of the bath before they recombine. In the following, we will distinguish the resulting low-energy state from a chemically doped metal, based on the properties of the optical conductivity.

Figure 3(a) shows the optical conductivity of the photodoped Mott insulator for various time delays after the excitation. The decrease of the kinetic energy due to dissipation leads to an increase of spectral weight according to the sum rule $\int d\omega \sigma(\omega, t) = -E_{\mathrm{kin}}(t)$. Nearly all added weight enters the Drude peak, while the weight W_{Hub} in the Hubbard band is reduced with respect to the undoped case. In fact, W_{Hub} measures only nearest neighbor short-time correlations, and with respect to this, photodoped and chemically doped states just look alike: The reduction of W_{Hub} is time independent and proportional to doping $\delta = \Delta d + \Delta h$, where here and in the following Δd and Δh denote the differences in the doublon and hole densities, respectively, with respect to the undoped insulator ($\delta \approx 2\%$ in Fig. 3).

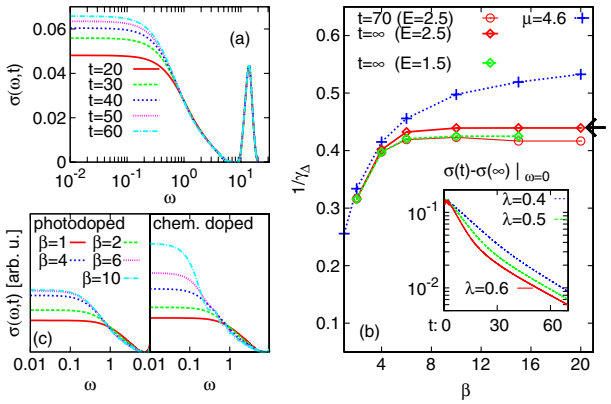

FIG. 3 (color online). (a) Optical conductivity $\sigma(\omega, t)$ [Eq. (2), $\Delta = 0.2$] at various times for the photodoped Mott insulator ($U = 14$, $\beta = 6$, $\lambda = 0.6$; pump: $E_0 = 2.5$). (b) Scattering time as a function of (bath) temperature for the chemically doped case ($\mu = 4.6$) and the photodoped case (both coupled to the same bath with $\lambda = 0.6$). Pump: $\Omega = 14$; excitation density $\delta \approx 0.8\%$ ($E_0 = 1.5$) and $\delta \approx 2\%$ ($E_0 = 2.5$). Circle symbols: Equation (3) taking $\bar{\sigma}(\omega, t)$ at $t = 70$. Diamonds: Equation (3) taking $\bar{\sigma}(\omega, t)$ from the extrapolation to $t = \infty$. Arrow: γ_Δ for a temperature quench ($\delta \approx 2\%$); see text. (Inset) $\bar{\sigma}(\omega, t) - \bar{\sigma}(\omega, \infty)$ for $\omega = 0$, where $\bar{\sigma}(\omega, \infty)$ is obtained from a fit $\bar{\sigma}(\omega, t) = \bar{\sigma}(\omega, \infty) + A \exp(-t/\tau)$. (c) Raw data for (b): $\sigma(\omega, t = 70)$ for the photodoped case (left, $E = 2.5$) and $\sigma(\omega)$ for the chemically doped case (right). Curves are normalized to unit weight.

The Drude peak and its width γ, on the other hand, can give a hint on whether or not coherent quasiparticles are being formed. Instead of γ, we compute the approximate measure

$$\gamma_\Delta = \bar{\omega}/\sqrt{\bar{\sigma}(\omega=0;\Delta)/\bar{\sigma}(\bar{\omega};\Delta)-1}, \quad (3)$$

which can be obtained from a finite time window (after relaxation of E_{kin}) and approaches γ for $\Delta \to 0$ and a Lorentz curve (we choose $\bar{\omega} = \Delta = 0.5$). Although the asymptotic behavior $\gamma \propto T^2$ is cut off below the scale Δ, γ_Δ still reveals the increase of the inverse scattering rate in the interesting temperature range where the chemically doped state enters the Fermi liquid regime [Fig. 3(b)]. In the photodoped state, in contrast, $1/\gamma_\Delta$ saturates at a smaller value for $T \lesssim 1/5$. Note that $\bar{\sigma}$ is not yet fully stationary at the largest simulation time $t = 70$. However, an exponential extrapolation, $\bar{\sigma}(t) = \bar{\sigma}(\infty) + A\exp(-t/\tau)$ (Fig. 3, inset) corrects γ_Δ only slightly, and moreover, it leads to a temperature-independent value [diamond symbols in Fig. 3(b)]. This finding, which is a central result of this Letter, is rather insensitive to the excitation density [see results for $E_0 = 1.5$, $\delta \approx 0.8\%$, and $E_0 = 2.5$, $\delta \approx 1$–2%, in Fig. 3(b)]. It shows that the photodoped state does not behave like a Fermi liquid upon lowering the temperature.

Further differences between photodoped and chemically doped states are evident in the spectral functions (Fig. 4): The occupied density of states $A^<(\omega,t) = (1/\pi)\mathrm{Re}\int_0^\infty ds e^{i\omega s}\langle c^\dagger(t+s)c(t)\rangle$, which for a quasisteady state is related to a time-resolved photoemission spectrum [24], evolves from a broad photoinduced distribution for small times into a peak concentrated at low frequencies. At the same time, the density of states, $A(\omega,t) = (1/\pi)\mathrm{Re}\int_0^\infty ds e^{i\omega s}\langle\{c(t+s)^\dagger, c(t)\}\rangle$, is not rigid as it would be for a noninteracting system, but it develops a feature at the lower edge of the upper Hubbard band (the lower Hubbard band is symmetric). This feature is different

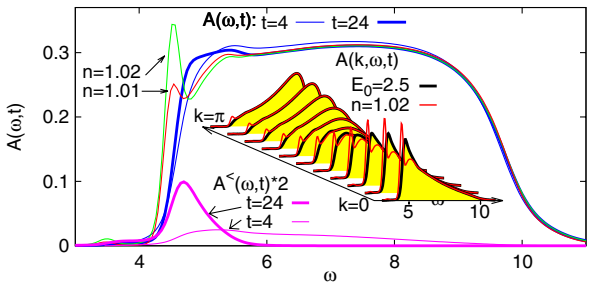

FIG. 4 (color online). Spectral function in the upper Hubbard band. $A(\omega,t)$, $A^<(\omega,t)$: photodoped, $U = 14$, $\beta = 15$, $\lambda = 0.6$; pump $\Omega = 14$, $E_0 = 2.5$ (excitation density $\Delta d = 0.01$). The curves labelled by $n = 1.01 = 1 + \Delta d$ and $n = 1.02 = 1 + 2\Delta d$ correspond to chemically doped states, where frequency axis is offset by $\Delta\omega = \mu$. Inset: Momentum-resolved $A_k(\omega)$ for various k and same parameters. Light red curves: Chemically doped case at $n = 1.02$; shaded curves: photodoped case.

from the quasiparticle peak of a chemically doped system, both when the density n of the latter is adjusted to the total number of photodoped carriers ($n - 1 = 2\Delta d$) or to the number of electronlike carriers ($n - 1 = \Delta d$). A closer look at the momentum resolved spectral function $A_k(\omega,t) = (1/\pi)\mathrm{Re}\int_0^\infty ds e^{i\omega s}\langle\{c_k(t+s)^\dagger, c_k(t)\}\rangle$ after the system has become nearly stationary ($t = 40$) reveals that this feature belongs to a relatively broad band of heavily scattered charge excitations (Fig. 4, inset).

It is also interesting to note that the photoinduced state is rather independent of the excitation procedure. To verify this fact, we have performed a similar numerical analysis as above, but now the system is initially prepared at high temperature ($\beta^* = 0.4$) and then suddenly coupled to a bath at lower temperature ($\beta = 10$). In this temperature quench, carriers in the system are of thermal origin rather than photoexcited, but the long-time behavior of γ_Δ nevertheless turns out to be the same as for the photodoped case [arrow in Fig. 3(b)].

For $U \gg v$, strong-coupling perturbation theory for the Hubbard model gives a possible interpretation of our results: Up to corrections of higher order in v/U, a Schrieffer-Wolff transformation brings the Hamiltonian (1) into a form $H_{U\gg v}$ which separately conserves both doublon and hole numbers [25]. While the chemically doped equilibrium state corresponds to the subspace without doublons or holes (t-J model), in nonequilibrium interesting dynamics can occur in different sectors of the Hilbert space, such as metastable superconductivity [26] or the strong-coupling prethermalization after an interaction quench [27]. Our results hence may suggest that the corresponding equilibrium state with equal density of both doublons and holes is a bad metal rather than a Fermi liquid in the investigated temperature range, in contrast to the case of pure electron or hole doping. Another possible interpretation would be that Fermi-liquid properties are reached only on a different (longer) time scale, which is not accessible by a short time extrapolation. Such a fundamentally different short and long time behavior has been observed at dynamical symmetry-breaking transitions [28,29].

In conclusion, we have demonstrated that the properties of photodoped and chemically doped Mott insulators are distinct on rather long times, even when photoinduced carriers can transfer their initially high kinetic energy to the environment before recombination occurs. A temperature-independent scattering time of the carriers is approached in the photodoped system, for temperatures where an electron or hole doped equilibrium system already behaves as a Fermi liquid. Experimentally, this results in a low mobility of photodoped carries, which could be seen in a terahertz study of the Drude part of photodoped metals. Good candidates to observe this physics in systems of dimension greater than one are cuprates, or organic charge transfer salts, which can be tuned over

the Mott transition by changing pressure (bandwidth) in equilibrium [30].

We thank J. Freericks, S. Kehrein, M. Kollar, Th. Pruschke, T. Oka, and N. Tsuji for useful discussions. We acknowledge support from SNF Grant No. PP0022-118866 and FP7/ERC starting Grant No. 278023.

[1] H. Okamoto, H. Matsuzaki, T. Wakabayashi, Y. Takahashi, and T. Hasegawa, Phys. Rev. Lett. **98**, 037401 (2007).
[2] S. Wall, D. Brida, S. R. Clark, H. P. Ehrke, D. Jaksch, A. Ardavan, S. Bonora, H. Uemura, Y. Takahashi, T. Hasegawa, H. Okamoto, G. Cerullo, and A. Cavalleri, Nat. Phys. **7**, 114 (2011).
[3] S. Iwai, M. Ono, A. Maeda, H. Matsuzaki, H. Kishida, H. Okamoto, and Y. Tokura, Phys. Rev. Lett. **91**, 057401 (2003).
[4] H. Okamoto, T. Miyagoe, K. Kobayashi, H. Uemura, H. Nishioka, H. Matsuzaki, A. Sawa, and Y. Tokura, Phys. Rev. B **82**, 060513 (2010).
[5] J. H. Davies and J. W. Wilkins, Phys. Rev. B **38**, 1667 (1988).
[6] R. Sensarma, D. Pekker, E. Altman, E. Demler, N. Strohmaier, D. Greif, R. Jördens, L. Tarruell, H. Moritz, and T. Esslinger, Phys. Rev. B **82**, 224302 (2010).
[7] P. Schmidt and H. Monien, arXiv:cond-mat/0202046.
[8] J. K. Freericks, V. M. Turkowski, and V. Zlatić, Phys. Rev. Lett. **97**, 266408 (2006).
[9] A. Georges, G. Kotliar, W. Krauth, and M. J. Rozenberg, Rev. Mod. Phys. **68**, 13 (1996).
[10] A. Amaricci, C. Weber, M. Capone, and G. Kotliar, Phys. Rev. B **86**, 085110 (2012).
[11] M. Eckstein and P. Werner, Phys. Rev. Lett. **107**, 186406 (2011).
[12] N. Tsuji, T. Oka, P. Werner, and H. Aoki, Phys. Rev. Lett. **106**, 236401 (2011).
[13] C. Aron, Phys. Rev. B **86**, 085127 (2012).
[14] Ph. Werner and M. Eckstein, Phys. Rev. B **86**, 045119 (2012).
[15] N. Tsuji, T. Oka, and H. Aoki, Phys. Rev. B **78**, 235124 (2008); Phys. Rev. Lett. **103**, 047403 (2009).
[16] M. Eckstein, M. Kollar, and P. Werner, Phys. Rev. B **81**, 115131 (2010).
[17] M. Eckstein and Ph. Werner, Phys. Rev. B **82**, 115115 (2010).
[18] M. Eckstein and Ph. Werner, Phys. Rev. B **84**, 035122 (2011).
[19] H. Keiter and J. C. Kimball, Int. J. Magn. **1**, 233 (1971); J. Appl. Phys. **42**, 1460 (1971); N. Grewe and H. Keiter, Phys. Rev. B **24**, 4420 (1981); Y. Kuramoto, Z. Phys. B **53**, 37 (1983).
[20] See Supplemental Material at http://link.aps.org/supplemental/10.1103/PhysRevLett.110.126401 for OCA results, and for a discussion of the influence of the density of states used within the DMFT self-consistency loop.
[21] W. Metzner and D. Vollhardt, Phys. Rev. Lett. **62**, 324 (1989).
[22] M. Eckstein and M. Kollar, Phys. Rev. B **78**, 205119 (2008).
[23] P. B. Allen, Phys. Rev. Lett. **59**, 1460 (1987).
[24] J. K. Freericks, H. R. Krishnamurthy, and T. Pruschke, Phys. Rev. Lett. **102**, 136401 (2009); M. Eckstein and M. Kollar, Phys. Rev. B **78**, 245113 (2008).
[25] A. B. Harris and R. V. Lange, Phys. Rev. **157**, 295 (1967).
[26] A. Rosch, D. Rasch, B. Binz, and M. Vojta, Phys. Rev. Lett. **101**, 265301 (2008).
[27] M. Eckstein, M. Kollar, and P. Werner, Phys. Rev. Lett. **103**, 056403 (2009).
[28] M. Heyl, A. Polkovnikov, and S. Kehrein, arXiv:1206.2505.
[29] N. Tsuji, M. Eckstein, and Ph. Werner, arXiv:1210.0133.
[30] M. Dumm, D. Faltermeier, N. Drichko, M. Dressel, C. Mézière, and P. Batail, Phys. Rev. B **79**, 195106 (2009).